



Phase constituents of Al-rich U–Mo–Al alloys examined by transmission electron microscopy

E. Perez^a, A. Ewh^a, J. Liu^a, B. Yuan^a, D.D. Keiser Jr.^b, Y.H. Sohn^{a,*}

^aAdvanced Materials Processing and Analysis Center, Department of Mechanical, Materials and Aerospace Engineering, University of Central Florida, Orlando, FL 32816, USA

^bIdaho National Laboratory, Idaho Falls, ID, USA

ARTICLE INFO

Article history:

Received 27 May 2008

Accepted 9 September 2009

ABSTRACT

To supplement the understanding of diffusional interactions involving Al-rich region of the U–Mo–Al system, alloys with composition 85.7Al–11.44U–2.86Mo and 87.5Al–10U–2.5Mo in at.%, were examined to determine the equilibrium phase constituents at 500 °C. These alloys were triple arc-melted, homogenized at 500 °C for 200 h, and water-quenched to preserve the high temperature microstructure. X-ray diffraction, scanning electron microscopy (SEM) with energy dispersive X-ray spectroscopy (XEDS), and transmission electron microscopy (TEM) with high angle annular dark field (HAADF) imaging via scanning transmission electron microscopy (STEM) were employed for the characterization. Alloy specimens for TEM/STEM were prepared using site-specific focused ion beam (FIB) in situ lift-out (INLO) technique. Despite the homogenization time and temperature, five different phases, namely fcc-Al solid solution, cubic-UAl₃, orthorhombic-UAl₄, hexagonal-U₆Mo₄Al₄₃ and diamond cubic-UMo₂Al₂₀, were observed. Based on U–Al, U–Mo and Al–Mo binary phase diagrams, previously proposed U–Mo–Al isotherms, and the solidification microstructure of these alloys, the Al-rich region of the equilibrium ternary isotherm at 500 °C was constructed. The fcc-Al solid solution, orthorhombic-UAl₄, and diamond cubic-UMo₂Al₂₀ which were determined to be the equilibrium phases in 85.7Al–11.44U–2.86Mo and 87.5Al–10U–2.5Mo alloys.

© 2009 Elsevier B.V. All rights reserved.

1. Introduction

U–Mo dispersion fuels in Al-alloys are being developed to fulfill the requirements of low enriched uranium in research reactors [1] under the Reduced Enrichment for Research Test Reactors (RERTR) program [2]. An understanding of phase constituents, thermodynamic parameters, growth kinetics and properties of the interaction layers that develop in the U–Mo–Al system [3–8] can provide optimized materials chemistry and processing parameters to improve the process-control, performance and service life of the U–Mo/Al fuel system. U–Mo alloys show promising results due to their high uranium density [1,9–11]. However, a significant interaction can take place between the U–Mo fuel and the Al matrix during fuel processing and irradiation. This interaction produces Al-rich phases with physical and thermal properties that can adversely affect the performance of the fuel system. The interdiffusion-controlled growth of layers that develop between the U–Mo fuel and the Al matrix can experience a significant volumetric expansion [12] that leads to fracturing. These interaction layers can also have lower thermal conductivities [13] than desired,

which can accelerate the rate of interaction between the U–Mo fuel and the Al-alloys, and other temperature-dependent deterioration modes of U–Mo monolithic/dispersion fuels, including swelling.

Several experiments have been carried out to determine the identity and growth rate of interaction layers using dispersion and monolithic fuel plates during irradiation [10,4–18]. Out-of-pile experiments have also been conducted in laboratory with depleted uranium (DU) alloys using dispersion and monolithic fuels [9,10] as well as diffusion couples [19–23]. In most cases, complex multiphase interaction layers have been observed to develop, and can include UAl₃, UAl₄, U₆Mo₄Al₄₃, UMo₂Al₂₀ [20–22,25] and an amorphous phase under irradiation [26,27].

The above studies have identified the phases from diffusional reactions requiring the assumption of local thermodynamic equilibrium and are complicated by other alloying additions in the Al-alloys that may influence the phase equilibria. In most diffusion studies, complex microstructures, including three-phase layers and elongated grains, have been observed.

Attempts to model the growth of the interdiffusion zone in diffusion couples have been made based on first principle calculations [28] and the observed behavior [29,30] of diffusion couples. In order to validate the assumption of local thermodynamic equilibrium in the interdiffusion zone and to determine the effect of alloying additions, the behavior of high purity U–Mo–Al diffusion

* Corresponding author. Tel.: +1 407 882 1181; fax: +1 407 882 1461.
E-mail address: ysohn@mail.ucf.edu (Y.H. Sohn).

couples must be correlated to that of the equilibrated U–Mo–Al compositions.

In this study, Al-rich U–Mo–Al alloys were cast and homogenized to determine the equilibrium phase constituents to clarify the phase equilibrium at 500 °C. The cast composition of two alloys, 85.7Al–11.44U–2.86Mo and 87.5Al–10U–2.5Mo in at.%, were selected considering typical average compositions for the interaction layers reported in literature [20,24,25]. The existing binary phase diagrams of U–Al, Mo–Al and U–Mo, results from other studies [14,16–24,26–28,32] and observations made in this study, were used to examine the Al-rich side of the U–Mo–Al ternary isotherm at 500 °C. Mazaudier et al. [15] made some recent contributions to a region near the one under consideration in this study based on diffusion couple experiments annealed at similar temperatures.

2. Experimental procedure

Alloys with nominal compositions 85.7Al–11.44U–2.86Mo and 87.5Al–10U–2.5Mo in at.%, hereinafter referred to as 85.7Al and 87.5Al, respectively, have been cast by arc melting of high purity Al, U and Mo. Each alloy was re-melted three times to ensure complete melting of each element in order to minimize macro-scale segregation. The alloys were then annealed at 500 °C for 200 h in an Ar atmosphere. One specimen, roughly 3 mm by 3 mm by 3 mm, was removed from each casting for this study. X-ray diffraction (XRD) patterns were collected for these alloys using a Rigaku™ D-MaxB diffractometer operating with Cu-K α radiation at 40 kV and 30 mA with a 1° divergence slit. Preferred crystallographic orientations were observed, presumably due to solidification process. Thus no quantitative analysis was carried out. For microstructural analysis, the specimens were mounted in epoxy, sectioned and metallographically polished down to 1 μ m using diamond paste. The microstructures of these alloys were then examined using a Hitachi™ S3500N scanning electron microscope (SEM) and a JEOL™ 6400F field-emission SEM. Backscatter electron (BSE) micrographs and standardless semi-quantitative (Genesis ver. 3.6, EDAX Inc.). X-ray energy dispersive spectroscopy (XEDS), using the ZAF correction method, were employed for microstructural and compositional analysis. Errors in accuracy may be expected in the XEDS measurements due to the assumptions made in the quantita-

tive standardless analysis. In this study, errors up to 3 at.% from the expected phase compositions were observed in the XEDS results.

Specimens for TEM were prepared with a focus ion beam (FIB) in situ lift-out (INLO) technique by using a FEI™ 200TEM. The specimens were selected from specific regions in the alloys to capture the phases observed by SEM. The samples were thinned to 100 nm in order to obtain electron transparency during TEM analysis. A FEI/Tecna™ F30 300 keV TEM/STEM, equipped with a Fischione™ HAADF detector and XEDS, was used for analysis of phase constituents and microstructure. Bright field imaging and selected area electron diffraction were used to carry the analysis.

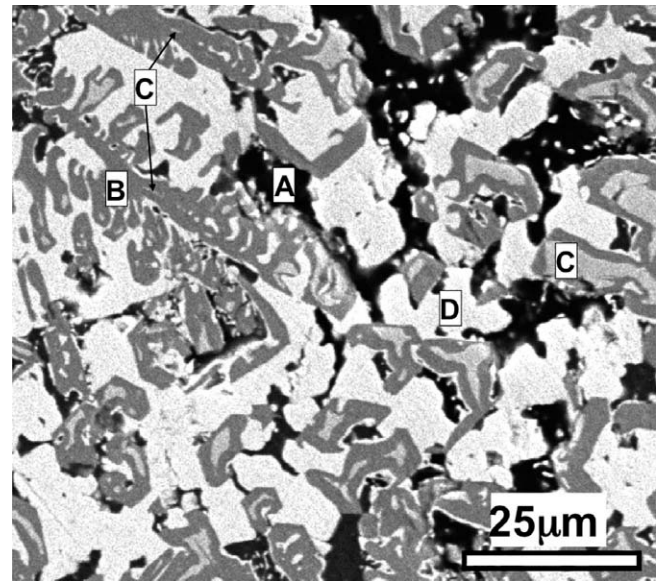


Fig. 2. Backscatter micrographs showing the typical microstructures of the 87.5Al alloy. Four different phases are visible based on images contrast.

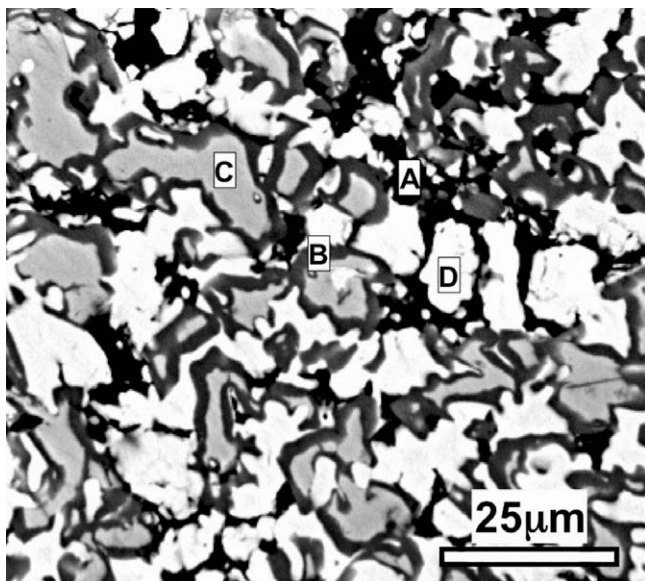


Fig. 1. Backscatter micrographs showing the typical microstructures of the 87.5Al alloy. Four different phases are visible based on images contrast.

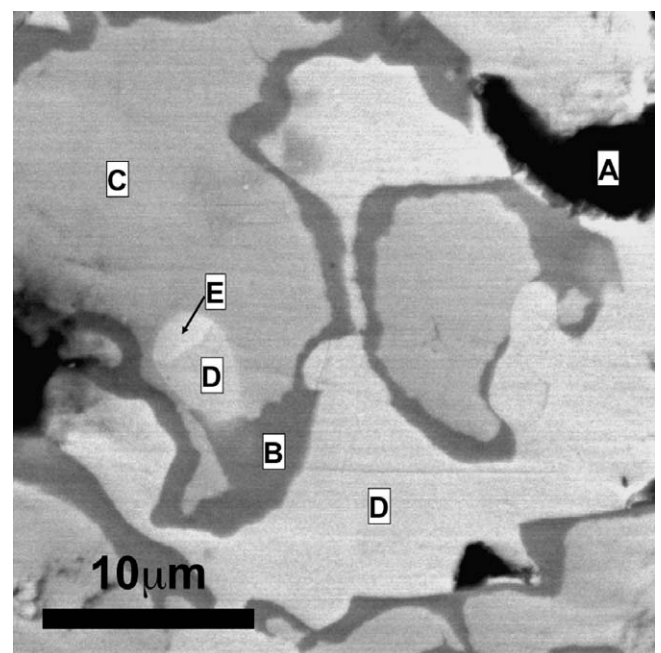


Fig. 3. Backscatter micrograph of the 85.7Al alloy showing a small precipitate phase observed in this alloy.

3. Results

Figs. 1 and 2 present typical BSE micrographs obtained from the 85.7Al and 87.5Al alloys, respectively. In total, five different phases were observed. This indicates that complete phase equilibrium was not achieved despite the homogenization at 500 °C for 200 h. Four of the phases, identified as regions A through D, are distributed in both alloys as shown in Figs. 1 and 2. The fifth phase, identified as region E in Fig. 3, is observed only in the 85.7Al alloy in extremely small quantities. Approximate compositional analysis for these phases (i.e., regions A through E) was conducted by XEDS on the

SEM. Table 1 reports the average composition of regions A through D determined based on collection of five minimum measurements per region. Only two measurements were carried out for the small residual phase (i.e., region E) shown in Fig. 3 due to its size and quantity. The standard deviations of the measured phase compositions, also reported in Table 1, demonstrate little variation in the compositions of the observed phases. The UAl_3 and UAl_4 phases exhibited little or no solubility for Mo.

Alloy specimens were prepared for TEM/STEM analysis via FIB-INLO for detailed examination of phase constituents. Fig. 4a shows a HAADF STEM micrograph of 85.7Al alloy. Based on electron

Table 1
Microstructural and compositional characteristics of the phases observed in the 85.7Al–11.44U–2.86Mo and 87.5Al–10U–2.5Mo alloys.

Alloy	Identified region	BSE appearance	Phase	Composition (at.%)		
				U	Mo	Al
85.7Al	A	Black	Al solid solution	2.1 ± 1.1	0.6 ± 0.5	97.4 ± 1.4
	B	Dark gray	UMo_2Al_{20}	5.2 ± 0.5	5.7 ± 0.6	89.1 ± 0.3
	C	Light gray	$U_6Mo_4Al_{43}$	12.2 ± 3.1	6.4 ± 3.2	81.3 ± 0.6
	D	White	UAl_4	18.0 ± 0.4	0.7 ± 0.4	81.3 ± 0.4
	E	Small residual	UAl_3	22.3 ± 0.4	0.7 ± 0.1	77.0 ± 0.5
87.5Al	A	Black	Al solid solution	0.9 ± 0.4	0.2 ± 0.1	98.9 ± 0.3
	B	Dark gray	UMo_2Al_{20}	4.8 ± 0.8	5.6 ± 0.9	89.5 ± 0.4
	C	Light gray	$U_6Mo_4Al_{43}$	10.5 ± 0.3	8.0 ± 0.6	81.6 ± 0.8
	D	White	UAl_4	18.2 ± 0.3	0.3 ± 0.1	81.5 ± 0.3

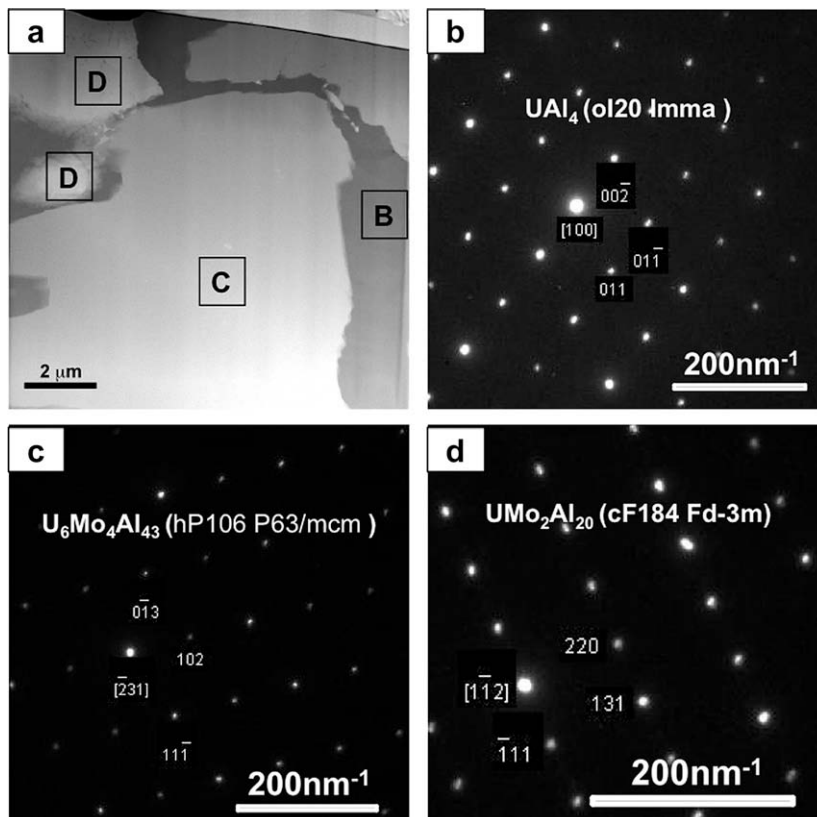


Fig. 4. (a) High angle annular dark field (HAADF) TEM image of the 85.7Al alloy and (b–d) electron diffraction patterns for the same alloy.

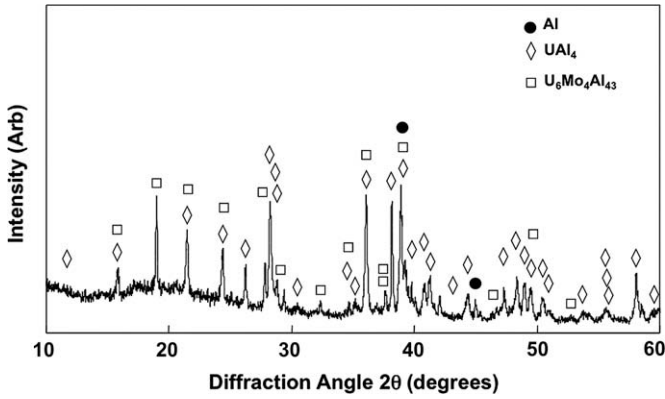


Fig. 5. X-ray diffraction patterns of 85.7Al.

diffraction patterns shown in Fig. 4b–d, and composition reported in Table 1, the three phases presented in Fig. 4a were identified as orthorhombic-UAl₄, hexagonal-U₆Mo₄Al₄₃ and diamond cubic-UMo₂Al₂₀. Despite the significant presence of overlapping peaks, XRD pattern from these alloys further suggests the presence of these phases as shown in Fig. 5 for the 85.7Al. The Al solid solution was not included in the TEM specimen for the 85.7Al alloy. Nevertheless, SEM/EDS and XRD analysis, both confirmed the presence of fcc-Al solid solution.

Fig. 6a shows a HAADF STEM micrograph of the 85.7Al alloy specimen that was specifically prepared by FIB-INLO to contain the small phase (i.e., region E in Fig. 3 and in Table 1). Based on electron diffraction, this phase was identified as the cubic-UAl₃ phase found in the binary U–Al system. The composition of this phase, as measured by XEDS and shown in Table 1, agrees well with the binary UAl₃ phase with little solubility for Mo.

Fig. 7 shows a HAADF STEM micrograph from the 87.5Al alloy specimen that contains fcc-Al, orthorhombic-UAl₄, and hexagonal-U₆Mo₄Al₄₃. These phase constituents are similar to those observed in 85.7Al alloy. The XRD pattern shown in Fig. 8 for the 87.5Al also suggests the presence of these major phase constituents, and shows the presence of diamond cubic-UMo₂Al₂₀ phase that was not presented in Fig. 5 for the 85.7Al alloy. The relative peak intensities of the U₆Mo₄Al₄₃ phase in the 87.5 alloy are significantly lower than those of the UAl₄ phase. As a result, some peaks may not be apparent in the collected pattern for the 87.5 alloy and may be more prevalent in the 85.7 alloy.

Comparison of Figs. 1 and 2 shows morphological differences in the microstructures of the alloys. The 87.5Al alloy contained a lar-

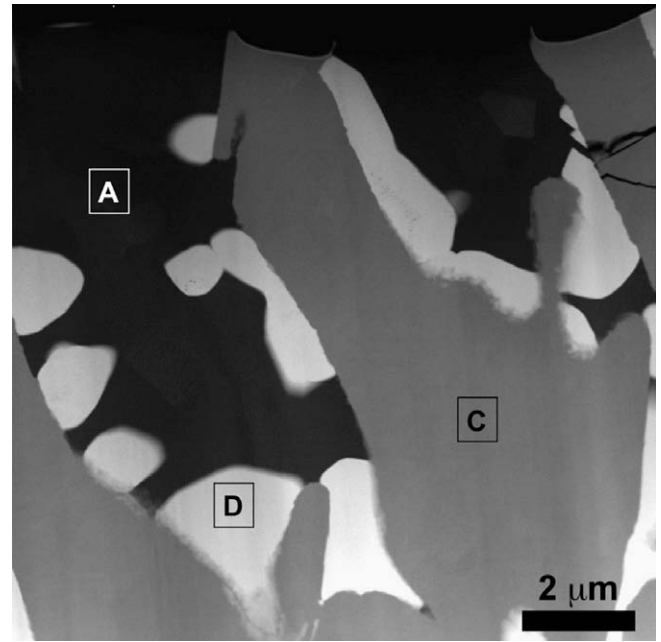


Fig. 7. High angle annular dark field (HAADF) TEM image of the 87.5Al alloy.

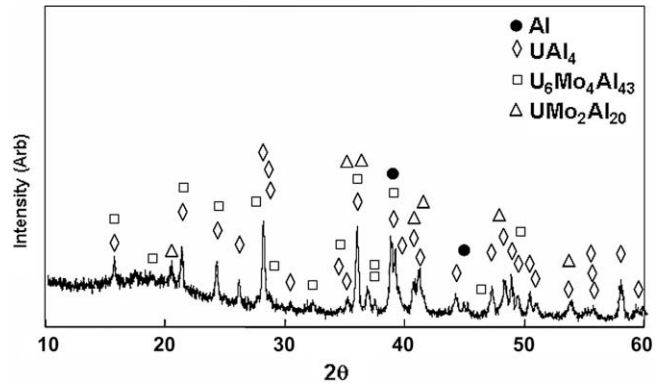


Fig. 8. X-ray diffraction patterns of 87.5Al.

ger volume fraction of Al solid solution and UMo₂Al₂₀, and lacked the UAl₃ phase. The volume fractions of the different phases vary between the two alloys. Nonetheless, the observed phases were found to be similar in the two alloys.

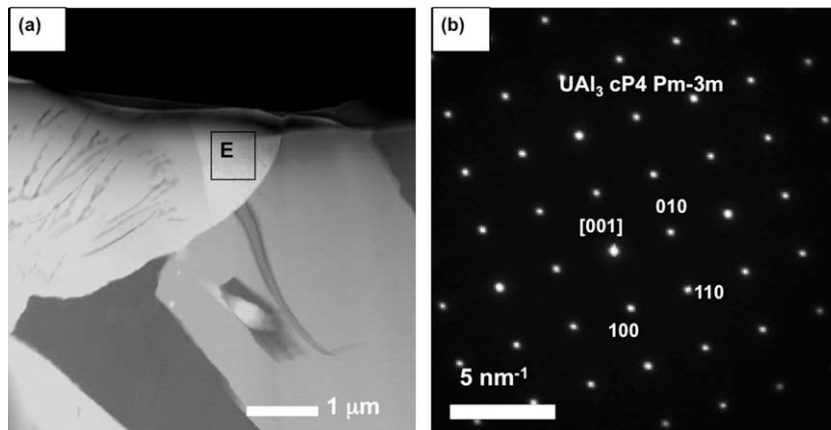


Fig. 6. (a) High angle annular dark field (HAADF) TEM image of the 85.7Al alloy, and (b) selected electron diffraction patterns for the same alloy.

4. Discussion

Interactions between U–Mo and Al-alloys have been shown to produce Al-rich binary and ternary compounds. The UAl_3 , UAl_4 , $\text{U}_6\text{Mo}_4\text{Al}_{43}$ and $\text{UMo}_2\text{Al}_{20}$ phases have been identified in the literature [14,17,18,10,19–23,25,26,28,31] and the possibility of other unidentified Al-rich phases has been also reported [9,32]. In order to clarify and supplement the data on the Al-rich side of the U–Mo–Al system, and to determine if any unidentified phases remain to be classified, the Al-rich portion of the U–Mo–Al ternary phase diagram at 500 °C, shown in Fig. 9, was constructed from the binary phase diagrams including ternary phases previously reported. The results of this study, discussed below, are compared to the literature [33] to confirm the Al-rich side of the ternary phase diagram.

The 85.7Al and 87.5Al alloy compositions were selected and produced based on the compositions of the Al-rich layer observed during diffusional interaction in U–Mo dispersion/monolithic fuels with Al-alloy matrix. All the different phases reported in these studies at or near 500 °C are expected to have developed in the alloys examined in this study. Five and four phases were observed in 85.7Al and 87.5Al alloys, respectively. According to Gibb's phase rule, only three phases are allowed under isothermal equilibrium condition for ternary alloys. The presence of extra phases indicates that these alloys did not achieve equilibrium, despite the homogenization at 500 °C for 200 h.

According to the U–Al binary phase diagram [32], and assuming for a moment that Mo, the minor alloying element in the system, does not play a significant role in the solidification path, the 85.7Al alloy would solidify via formation of first UAl_2 , followed by UAl_3 and then ($\text{UAl}_4 + \text{Al}$) phases at 500 °C. The 87.5 Al alloy would solidify via formation of UAl_3 , and then ($\text{UAl}_4 + \text{Al}$) phases only. Upon annealing, the phase constituents of these alloys would evolve towards equilibrium containing only the UAl_4 and Al solid solution phases. This study did not observe any UAl_2 phase, and found a very small amount of UAl_3 phase locally in the 85.7Al alloy only. The presence of UAl_3 phase is then most likely a result of incomplete homogenization and/or microsegregation. Therefore, based on the U–Al binary phase diagram, and the amount of fcc-Al and UAl_4 phases observed, we determine

that the fcc-Al and UAl_4 phases are equilibrium phases in the 87.5Al and 85.7Al alloys.

The $\text{U}_6\text{Mo}_4\text{Al}_{43}$ and $\text{UMo}_2\text{Al}_{20}$ phases observed in both alloys are the result of Mo additions into the U–Al system. Figs. 1 and 2 show that the $\text{U}_6\text{Mo}_4\text{Al}_{43}$ is generally surrounded by $\text{UMo}_2\text{Al}_{20}$. In agreement with this study, Mazaudier et al. noted that the UAl_4 and $\text{U}_6\text{Mo}_4\text{Al}_{43}$ phases never coexist in diffusion couples of U–Mo vs. Al-alloys. On Fig. 3, the phases come into contact in the presence of the UAl_3 phase; this is expected to be an artifact of the inhomogeneity from casting.

The development of the UAl_3 and UAl_4 phases in the alloys requires that Mo be rejected from these two Mo-depleted phases to produce a Mo enriched phase. The $\text{UMo}_2\text{Al}_{20}$ phase is slightly higher in Al and Mo content than the $\text{U}_6\text{Mo}_4\text{Al}_{43}$. Thus, based on sufficient Al content, presence of Mo, and microstructure of the alloys, we determine that the $\text{UMo}_2\text{Al}_{20}$ phase is likely the equilibrium phase for the alloys examined in this study.

In agreement with the results of Palancher et al. [34], Table 1 reports that all measured compositions of the phases in the alloys had very little variation. The solubility limits for the elements in the phases were not accurately determined, but the phases observed in these alloys have well defined compositions with little variation. Although the UAl_3 phase may not be an equilibrium phase in these alloys, both the UAl_3 and UAl_4 phases showed little or no solubility for Mo.

Other previously unidentified phases were not observed in the two alloys examined. Previous studies [9,10,19–23] reported the probability of unidentified Al-rich phases within the multiphase interdiffusion layers. The Al-rich phases observed in the diffusion couple experiments carried out at or near 500 °C may contain various mixture of cubic- UAl_3 , orthorhombic- UAl_4 , hexagonal- $\text{U}_6\text{Mo}_4\text{Al}_{43}$ and diamond cubic- $\text{UMo}_2\text{Al}_{20}$ phases, depending on diffusion path (e.g., composition path) as a function of terminal alloy compositions. Other unknown phases are not expected to develop in diffusion couples or in out-of-pile dispersion/monolithic fuel experiments of similar composition.

In the ternary isothermal phase diagram, the 85.7Al and 87.5Al alloys should lie in a three-phase region composed of Al solid solution, UAl_4 and $\text{UMo}_2\text{Al}_{20}$ phases, as shown in Fig. 9. The ternary isothermal phase diagram shown in Fig. 9 was drawn from the results of this study and data in the literature. It is in very good agreement with the one proposed by Mazaudier et al. [15], with the exception that the solubility limits of the two and three-phase regions are reduced based on the EDS results in Table 1, that show little variation in compositions of the phases. The accuracy of the EDS data collection may contain some error based on the nature of the process, but the EDS precision can be used to, at least, qualitatively measure compositional variations within a given phase.

5. Summary

Alloys with nominal compositions 85.7Al–11.44U–2.86Mo and 87.5Al–10U–2.5Mo (at.%) have been examined using XRD, SEM/EDS and TEM/STEM for identification of phase constituents and analysis of microstructure. The fcc-Al solid solution, cubic- UAl_3 , orthorhombic- UAl_4 , hexagonal- $\text{U}_6\text{Mo}_4\text{Al}_{43}$ and diamond cubic- $\text{UMo}_2\text{Al}_{20}$ phases were observed. Based on relevant binary phase diagrams, literature data and the microstructure of the alloys, fcc-Al solid solution, orthorhombic- UAl_4 , and diamond cubic- $\text{UMo}_2\text{Al}_{20}$ phases were determined to be in equilibrium at 500 °C for these alloys. A ternary isothermal phase diagram at 500 °C for the Al-rich side of the phase diagram was constructed including the hexagonal- $\text{U}_6\text{Mo}_4\text{Al}_{43}$, which is not considered as the equilibrium phase for the alloys examined. No other Al-rich equilibrium phase was observed near the compositional range.

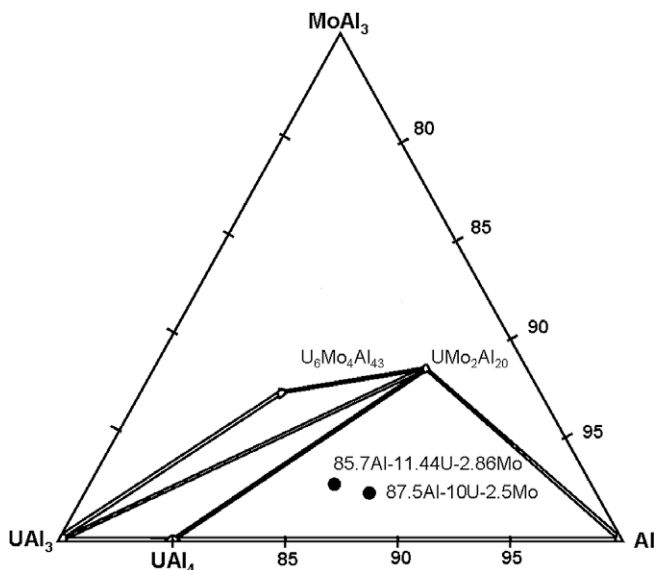


Fig. 9. Partial equilibrium ternary phase diagram for the U–Mo–Al system for the 500 °C isotherm.

Acknowledgements

This work was financially supported by Idaho National Laboratory (Contract No. 00051953) under the operation of US Department of Energy – Battelle Energy Alliance, LLC (DE-AC07-05ID14517). Additional financial support from CAREER Award of National Science Foundation (DMR-0238356) is gratefully acknowledged by the author, Yong-ho Sohn. Author, Ashley Ewh, an undergraduate research assistant sincerely appreciates the financial support of the Goldwater scholarship. Any opinions, findings, and conclusions or recommendations expressed in this manuscript are those of the authors and do not necessarily reflect the view of the National Science Foundation.

References

- [1] D.D. Keiser Jr., S.L. Hayes, M.K. Meyer, C.R. Clark, *JOM* 0 (2003) 55.
- [2] Federal Register, Rules and Regulations, vol. 51(37), February 25, 1986.
- [3] F. Muhammad, A. Majid, *Ann. Nucl. Energy* 35 (2008) 1720–1731.
- [4] S.H. Lee, J.M. Park, C.K. Kim, *Int. J. Thermophys.* 28 (5) (2007) 1578, doi:10.1007/s10765-007-0212-0.
- [5] H.J. Ryu, Y.S. Kim, G.L. Hofman, J.M. Park, C.K. Kim, *J. Nucl. Mater.* 358 (2006) 52.
- [6] R. Ahmed, Aslam N. Ahmad, *Ann. Nucl. Energy* 32 (2005) 29.
- [7] R. Ahmed, Aslam N. Ahmad, *Ann. Nucl. Energy* 32 (2005) 1100.
- [8] S.H. Lee, J.C. Kim, J.M. Park, C.K. Kim, S.W. Kim, *Thermophysics* 24 (5) (2003) 1355.
- [9] H.J. Ryu, Y.S. Han, J.M. Park, S.D. Park, C.K. Kim, *J. Nucl. Mater.* 321 (2003) 210.
- [10] S.L. Hayes, M.K. Meyer, G.L. Hofman, R.V. Strain, in: *Proceedings of the International Meeting on RERT, October 18–23, Sao Paulo, Brazil, 1998*.
- [11] J. Snelgrove, G.L. Hofman, M.K. Meyer, C.L. Trybus, T.C. Wiencek, *Nucl. Eng. Des.* 178 (1997) 119.
- [12] D.B. Lee, K.H. Kim, C.K. Kim, *J. Nucl. Mater.* 250 (1997) 79.
- [13] G.L. Hofman, M.K. Meyer, Y.-M. Park, in: *Proceedings of the International Meeting on RERT, October 1–6, Las Vegas NV, 2000*.
- [14] H. Palancher, N. Wieschalla, P. Martin, R. Tucoulou, C. Sabathier, W. Petry, J.F. Berar, C. Valot, S. Dubois, *J. Nucl. Mater.* (2009), doi:10.1016/j.jnucmat.2008.12.032.
- [15] F. Mazaudier, C. Proye, F. Hodaj, *J. Nucl. Mater.* 377 (2008) 476.
- [16] N. Wieschalla, A. Bergmaier, P. Böni, K. Böning, G. Dollinger, R. Großmann, W. Petry, A. Röhrmoser, J. Schneider, *J. Nucl. Mater.* 357 (2006) 191.
- [17] A. Leenaers, S. Van den Berghe, E. Koonen, C. Jarousse, F. Huet, M. Trotabas, M. Boyard, S. Guillot, L. Sannen, M. Verwerft, *J. Nucl. Mater.* 335 (2004) 39.
- [18] K.H. Kim, J.M. Park, C.K. Kim, G.L. Hofman, M.K. Meyer, *Nucl. Eng. Des.* 211 (2002) 229.
- [19] D.D. Keiser Jr., *Def. Diff. For.* 266 (2007) 131.
- [20] E. Perez, N. Hotaling, A. Ewh, D.D. Keiser, Y.H. Sohn, *Def. Diff. For.* 266 (2007) 149.
- [21] C.K. Varela, M. Mirandou, S. Aricó, S. Balart, L. Gribaudo, in: *Proceedings of the RRFM and IGORR, March 11–15, Centre de Congrès, Lyon, France, 2007*, p. 135.
- [22] M.I. Mirandou, S.N. Balart, M. Ortiz, M.S. Granovsky, *J. Nucl. Mater.* 323 (2003) 29.
- [23] D. Subramanyam, M.R. Notis, J.I. Goldstein, *Metall. Trans. A* 16A (1985) 589.
- [24] T.K. Bierlein, D.R. Green, *Nucl. Sci. Eng.* 2 (1957) 778.
- [25] F. Mazaudier, C. Proye, F. Hodaj, in: *Proceedings of the RRFM, April 30–May 3, Sofia, Bulgaria, 2006*, p. 87.
- [26] D.D. Keiser Jr., C.R. Clark, M.K. Meyer, *Scr. Mater.* 51 (2004) 893.
- [27] H.J. Ryu, Y.S. Kim, G.L. Hofman, *J. Nucl. Mater.* (2009), doi:10.1016/j.jnucmat.2009.01.306.
- [28] S. Van den Berghe, W. Van Renterghem, A. Leenaers, *J. Nucl. Mater.* 375 (2008) 340.
- [29] J.E. Garces, A.C. Marino, G. Bozzolo, *Appl. Surf. Sci.* 219 (2003) 47.
- [30] X.C.D. Olander, *J. Nucl. Mater.* 383 (2009) 201.
- [31] A. Soba, A. Denis, *J. Nucl. Mater.* 360 (2007) 231.
- [32] M.K. Meyer, G.L. Hofman, S.L. Hayes, C.R. Clark, T.C. Wiencek, J.L. Snelgrove, R.V. Strain, K.H. Kim, *J. Nucl. Mater.* 304 (2002) 221.
- [33] M.E. Kassner, P.H. Adler, M.G. Adamson, D.E. Peterson, *J. Nucl. Mater.* 167 (1989) 160.
- [34] H. Palancher, P. Martin, V. Nassif, R. Tucoulou, O. Proux, J.-L. Hazemann, O. Tougait, E. Lahéra, F. Mazaudier, C. Valot, S. Dubois, *J. Appl. Cryst.* 40 (2007) 1064.